Design of Low-Profile Tactile Actuator with Rich Vibrotactile Stimulation For Wearable Applications

1st Georgios Korres
Engineering Department
New York University, Abu Dhabi
United Arab Emirates
george.korres@nyu.edu

2nd Mohamad Eid
Engineering Department
New York University, Abu Dhabi
United Arab Emirates
mohamad.eid@nyu.edu

***Abstract*—Vibrotactile stimulation is becoming more popular in haptic applications due to its simplicity, cost-effectiveness, and the ability to be used in wearable/flexible devices. Traditional vibrotactile actuators are either low-cost with limited expressiveness of vibration cues or high-cost with great expressiveness. We designed, characterized, and perceptually evaluated a low-profile, low-cost vibrotactile actuator that can control frequency and intensity of vibration independently. The actuator characterization demonstrated its ability to display frequencies in a perceptually flat response for the frequency band (110-300 Hz). Furthermore, the vibration intensity can be controlled independently in the same frequency band (110-300Hz), producing a flat response. A psychophysics experiment is conducted to validate the perceptual capabilities of the actuator. It is found that the actuator can display perceptually distinct stimulation across the defined frequency and intensity bands. The proposed actuators can be used to develop ubiquitous vibrotactile stimulation with high expressivity at low cost.**

***Index Terms*—haptics, actuator, wearables, design**

I. Introduction

Vibrotactile stimulation is among the most common ways of eliciting haptic information in contemporary means of communication and a rising technology to enable physical yet simple feedback in human computer interaction [1]. Vibrotactile stimulation is common in many devices and applications fields such as mobile phones, tablets, wearable devices, medical, military, entertainment and navigation applications [2] [3]. It can be mediated through direct contact using vibrotactile actuators or in mid-air using focused ultrasound or laser stimulation [4] [5] [6]. The wide range of applications in which vibrotactile stimulation is essential dictates the existence of a wide variety of vibrotactile actuators [7].

With regards to the contact-based vibrotactile stimulation for wearable applications, the ideal actuator needs to be small in size to fit in wearable devices, low-cost and power efficient, and deliver a wide range of perceivable cues by independently controlling frequency and intensity of vibration. As we will see more comprehensively in the next section, none of the commercially available actuators can satisfy all of the aforementioned specifications - there is always a tradeoff between expressiveness and cost. In this paper, we propose a low cost, 3D printed vibrotactile actuator that can adequately satisfy all the specifications mentioned above. We designed, simulated, developed and characterized a small form factor vibrotactile actuator with a 5 mm profile, capable of delivering a wide range of, independently controlled vibration frequencies and intensities with a power consumption of less than one Watt of power and with an approximate cost of $10.

The rest of the paper is organized as follows: we present an overview of the related work on the development of contact-based vibrotactile actuators for wearable applications in section II. The design, simulation and development of the actuator is introduced in section III. The actuator characterization is presented in section IV. In section V, a psychophysical experiment is presented. Sections VI presents the experiment findings along with a discussion about the derived conclusions. Section VII summarizes the study and provides perspectives for future work.

II. Related Work

Vibrotactile actuation technologies can be generally classified into four categories: Eccentric Rotating Mass (ERM), Linear Resonant Actuator (LRA), Piezo actuators, and coil-based actuation [8]. Other technologies such as solenoid actuators [9] or flexible and bendable actuators (in order to create an arbitrary shape of tactile feedback surface) [10], are also available. However, these technologies are not as common in vibrotactile actuators and thus will not be considered for comparison.

ERMs are comprised of an off-center rotating mass which, as it spins, creates an omni-directional vibration which propagates throughout the device. However, due to the construction of the ERM, the ability to create sophisticated vibrotactile cues is limited. The frequency and amplitude of vibration are coupled together to the input-control voltage, leaving just one variable to play with to create different effects. Even though they are low-cost, ERMs are characterized by a slower speed and response time, and thus are less favorite for real-time applications (30-60 millisecond range) [11].

The LRA use a magnet attached to a spring, surrounded by a coil and housed in a casing. The magnet oscillates in a linear fashion up to a resonance frequency, which allows the driver to operate at a lower power-consumption rate (compared to ERMs) [12]. The technology is low-cost, however, one limitation is that vibration is locked in at the resonance frequency so efficiency and performance drops off considerably

978-1-7281-2355-4/19/$31.00 ©2019 IEEE

as frequency moves outside the resonant band. With respect to response time, LRAs are considered slow and thus less suited for real-time haptic interaction.

A piezo actuator involves a thin strip or a round disk that goes from flat to bent and back, thus creating vibration by applying a voltage across its ends. Piezo-based vibration technology is not bound by any frequency or intensity constraints, allowing the designer to create profiles not attainable by LRAs and ERMs. However, they require extremely high peak-to-peak voltage (100-200 Volts) to be driven through the device, which significantly worsens the design complexity, safety, and cost [13]. On the other hand, they are characterized by low response time, which makes them suitable for real-time interactions.

Coil-based actuators utilize a coil that encloses a movable magnet [14]. An on/off current signal flowing into the coil produces vibration of the magnet due to on/off magnetic field applied to the magnet. Notable examples are the C2 tactor [15] and the Haptuator [9]. These actuators are significantly more expensive than ERMs or LRAs. Therefore, our proposal is to develop low-cost, high expressiveness coil actuators for vibrotactile applications.

In comparison to existing technologies, the proposed design offers a low cost, high expressiveness, low power consumption profile, and compact size. Table 1 shows a summary of the comparison of the proposed design with common vibrotactile actuation technologies. One limitation of the proposed design is the relatively lower acceleration that it provides, however, this is clearly above the perception thresholds for the entire human body (less than 0.1g) [16].

TABLE I
QUALITATIVE COMPARISON WITH COMMON VIBROTACTILE ACTUATION TECHNOLOGIES

Technology	Cost	Power	Full Control	Speed	Profile	Acc.
ERM	Low	Medium	No	Slow	Low	Medium
LRA	Low	Medium	No	Slow	Low	Medium
PZT	High	Medium	No	Fast	Low	Medium
Coil-based	High	High	Yes	Fast	Medium	Medium
Proposed	**Low**	**High**	**Yes**	**Fast**	**Low**	**Medium**
Ideal	**Low**	**Low**	**Yes**	**Fast**	**Low**	**High**

III. ACTUATOR DESIGN AND SIMULATION

A. Design

The proposed actuator comprises five main parts, as shown in Figure 1: the lower case, the moving magnet, the membrane, the coil and the upper case (cap). The lower case is a 4 mm height structural ground that supports the membrane and hosts the coil of the actuator. The next component is the coil. Since the main objective of this design was to keep the actuator's profile as low as possible, a flat (0.5 mm height) spiral coil is utilized. The coil is placed on the circular edge of lower case, 2 mm above the coil. The membrane is resting stressed by the upper case. The membrane is cut to shape by sheet of Nitrile rubber, with a thickness of 0.08 mm. The moving mass consists of a small coin type Neodymium magnet with a thickness of 2 mm and 9 mm of diameter. The membrane-magnet coupling is also protected by the cap of the actuator which is also part of the case. The total thickness of the actuator is around 5 mm. Figure 2 shows a snapshot of the assembled actuator.

Another novelty of this design is that the magnet is the moving part on the actuator whereas the coil remains static, unlike voice coil actuators where the magnet is the stator and the coil is the moving part. This opened the door for keeping an even lower profile and at the same time eliminated the need for high precision machined parts due to the axisymmetric nature of the design.

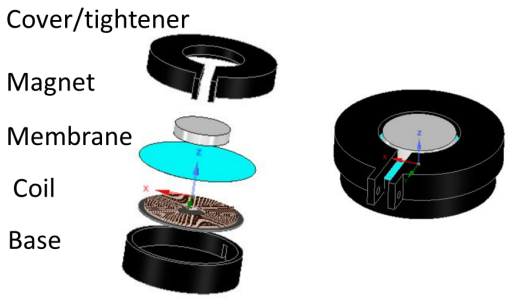

Fig. 1. (left) Structure of the proposed actuator, (right) 3D model of the actuator.

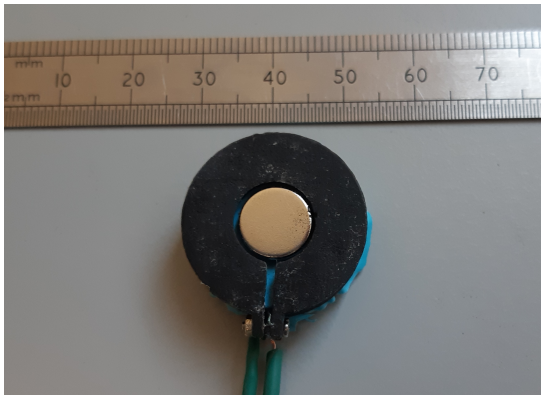

Fig. 2. A prototype of the vibrotactile actuator next to a ruler for scale

B. Magnetostatic Analysis

Before developing the actuator, several simulations were held in order to characterize the intensity and properly tune the actuator to the appropriate frequency range. In order to calculate the magnetic force generated when current flows through the coil, a magnetostatic analysis was held using ANSYS software. In magnetostatic analysis, the magnetic field is calculated under a steady current. The magnetostatic equations are derived from Maxwell's equations under the assumption that the charges are either fixed or move with a steady current J. Therefore, Maxwell's equations are split into two pairs of equations: two equations for the electric field (electrostatics) and two equations for the magnetic field (magnetostatics) . For a magnetostatic analysis, when introducing the magnetic

vector potential (MVP) $\mathbf{A}$ such that $\mathbf{B} = \nabla \times \mathbf{A}$ then the magnetostatic response approximation of Maxwell's equations for a steady current density distribution $\mathbf{J}$ is given by:

$$\nabla \times \left(\mu^{-1} \cdot \nabla \times \mathbf{A}\right) = \mathbf{J} \tag{1}$$

where $\boldsymbol{\mu}$ is the magnetic permeability tensor which relates the magnetic flux density $\boldsymbol{B}$ to the magnetic field $\boldsymbol{H}$ through the constitutive equation $\boldsymbol{B} = \boldsymbol{\mu} \cdot \boldsymbol{H}$.

The variation formulation of equation 1 which will be used by Finite Elements solver is given by:

$$\int_V \nabla \times \delta\mathbf{A} \cdot \left(\mu^{-1} \cdot \nabla \times \mathbf{A}\right) dV = \int_V \delta\mathbf{A} \cdot \mathbf{J} dV + \int_S \delta\mathbf{A} \cdot \mathbf{K} dS \tag{2}$$

where $\delta\mathbf{A}$ is the variation of MVP and $\mathbf{K}$ is the tangential surface current density which is applied at external surfaces.

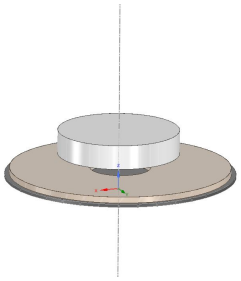

Fig. 3. The Magnetostatic model includes only the moving magnet and the coil

Figure 3 shows the 3D model used in the magnetostatic analysis. Four materials were used in this analysis: the Neodymium N42 (NdFeB) alloy with a residual induction of about 1300 mT and a coercive force of 955 KA/m to simulated the Neodymium magnet, a flat cooper disk of 0.5 mm thickness and 19 mm of diameter, 40 concentric turns and a cross sectional area of 3.3 mm^2 to model the coil as a stranded conductor, a soft magnetic ferrite core material which was located below the coil and surrounding air.

The force, which is generated by the coil and applied through the magnet, is calculated as the difference between the magnetostatic force generated from 700mA of current flowing through the coil and zero current flow. The force is calculated to around 0.123 N.

C. Frequency Response Analysis

The steady state response of the structure across a frequency range of 100 Hz to 300 Hz is performed while calculating the force acting on the moving mass of the actuator. However, this calculation is done under the assumption that the actuator is acting on the human's skin, so a simple model of the skin must be used in the frequency response analysis. A unidimensional spring damper model is used to model the skin with a stiffness value varying from 500 N/m to 800 N/m and a damping value of 0.28 N/ms to 0.845 N/ms [17]. The spring-damper skin model was coupled with the rest of the actuator model by connecting the first end of the spring-damper skin model to the center of the upper surface of the Neodymium magnet and the other end to the ground. The 3D model is meshed as shown in Figure 4.

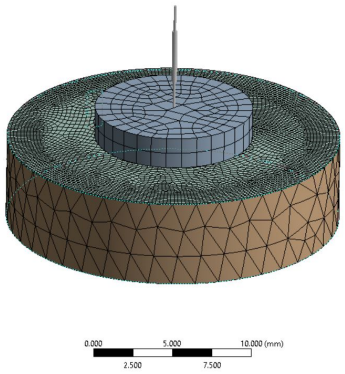

Fig. 4. The mesh of the actuator resulting about 6200 finite elements with 40k nodes

Dirichlet boundary conditions were set on the lower surface of the actuator's case to act as fixed support while the sinusoidal loading force was set to the upper surface of the neodymium magnet (Figure 5). Note that the maximum intensity of the sinusoidal loading force was derived from the magnetostatic analysis.

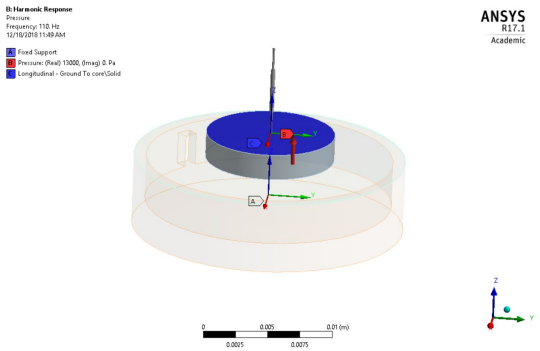

Fig. 5. Boundary conditions, loads and connections for the frequency response analysis

The frequency response was calculated in the range between 110 Hz to 300 Hz with 40 solution intervals on which the force acting on the skin and the maximum displacement of the actuator along Z axis were calculated (Figures 6 top and bottom plot respectively).

IV. Actuator Characterization

The 3D modeled parts of the actuator were printed and the actuator was assembled in accordance with the design specifications. In order to verify the actuator performance, a characterization experiment is conducted to measure its frequency response across a voltage range between 1 and 3 Volts. The experimental setup is presented in Figure 7. In order to measure the intensity of vibration, an ADXL335 analog

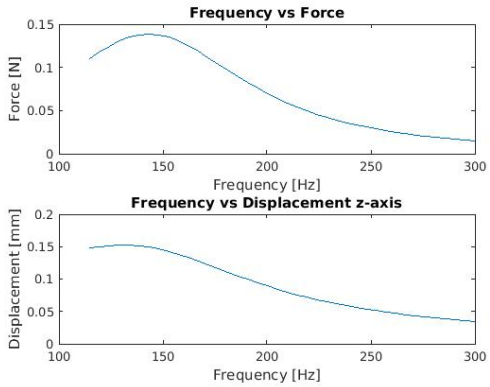

Fig. 6. Top: The force response exerted on the skin (this graph can be compared to the characterization plot of Figure 8). Bottom: the displacement response of the actuator.

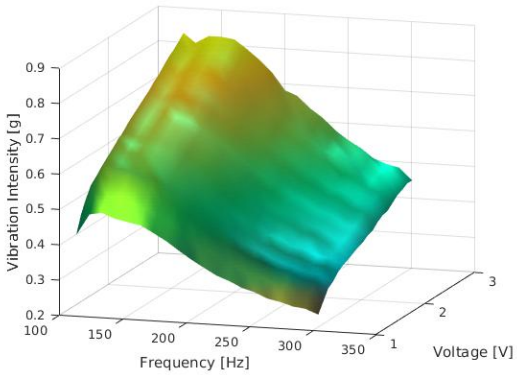

Fig. 8. The actuator characterization plot. It shows the response of the intensity of vibration for different voltage levels.

accelerometer was coupled on top of the actuator and probed to calculate the FFT of the accelerometer's output using an MSOX2024A Digital oscilloscope. The accelerometeractuator pair was resting on damping foam to filter any other sources of vibrational noise. The actuator's frequency was driven by an 33521A Arbitrary Signal Generator and the intensity of the signal was controlled through an N-Channel MOSFET from a DP831 digital power supply unit. All the instruments were connected to a laptop through USB ports where a MATLAB script controlled the instruments and the acquisition of data from the oscilloscope. The script was set at an initial voltage, then sweeping through a frequency range between 110 Hz and 300 Hz, acquiring the peak point of the accelerometer's response and then loop through the same procedure by increasing the voltage by 0.1 Volts.

Figure 8 shows the characterization of the proposed design. The surface plot shows the response of the actuator against frequency and voltage inputs. On the vertical axis, the vibration intensity is measured in multiples of gravitational acceleration [g] and the two other axes are the frequency and the intensity dimensions. It is clear from Figure 8 that a reasonable range of frequency (110-300 Hz) and intensity (more than 0.4g) make this actuator suitable for most vibrotactile stimulation applications.

Finally, we also measured the transient response of the vibrotactile actuator in order to determine the suitability of the design for real-time applications (short pulse vibrotactile application where fast transient response is desired). As show in figure 9, the transient response of the actuator at 300 Hz frequency is about 5 ms. The actuator needs approximately 2 cycles of operation to reach the steady state response which for vibrotactile stimulation applications, where the stimulation duration is on average 50 ms or higher [11], is considered to be satisfactory.

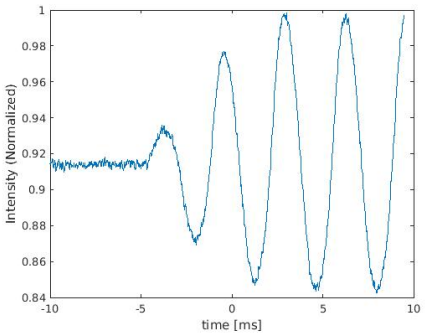

Fig. 9. The normalized transient response of the transducer at 300 Hz

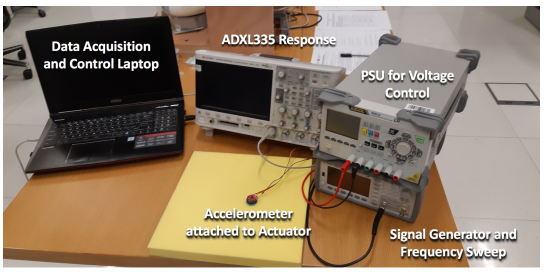

Fig. 7. The experimental setup that was used to characterize the actuator. All the components of the setup are discussed extensively in the text.

V. Perceptual Characterization Study

After the frequency/intensity characterization of the proposed design, the perceptual characteristics of the actuator are studied using a psychophysical experiment. In addition to validating that the operation frequency/intensity bands are perceivable, the objective of this study is to verify if users are capable of perceiving changes in frequency and intensity independently.

A total of 15 subjects participated in this study, which was approved by the IRB committee of New York University Abu Dhabi (IRB: 133-2018). All participants gave their written consent for this study before starting the experiment. Participants used their non-dominant hand for the vibrotactile perception and their dominant hand for controlling the mouse (to interact with the interface).

A. Experimental setup and procedure

A signal generator was used to control the frequency of the stimulation and its intensity was driven from a laboratory power supply as in the aforementioned characterization study. The actuator was attached firmly to the lower palmar region of the users' hand closer to the wrist. Two Matlab scrips were developed to drive the experiment, one for the intensity transitions and the other for the frequency transitions.

The experimental procedure was designed as follows: the stimulation space for the intensity was divided into three regions: low (0.3g), medium (0.5g) and high (0.7g), during which the frequency was kept steady at 200 Hz. The duration for the vibrotactile stimulation was kept constant at 1 second. The transitions in intensity could be increasing (when the second stimulation intensity is larger than the first stimulation intensity), decreasing (when the intensity of the second stimulation for smaller than the first stimulation) or the same (when the intensity is unchanged). The sequence of 9 combinations (from low/medium/high to low/medium/high) is presented in random order in order to counter-balance any learning biases. A simple graphical user interface prompted the user to click on a button on the screen to start the reference stimulation, then another message instructed the user to start the second stimulation according to the transition scheme. Finally, the user had to answer whether the intensity was increased, decreased or stayed the same. The space of 9 transitions was randomly shuffled and repeated three times resulting in 27 data-points on which the answers of the users and the response time of the users were recorded. The same procedure was followed for the frequency experiment with the intensity remaining steady this time at 0.5g while the frequency changing between low (110 Hz), medium (200 Hz) and high (300 Hz).

B. Results

The average and standard deviations of the recognition rates for all the frequency/intensity transitions are calculated. A summary of the results is shown in Table II. The recognition rate for changes in intensity was 76.5% (with a standard deviation of 2.52%) whereas the recognition rate for changes in the frequency was 77.77% (with a standard deviation of 3.46%). This result clearly demonstrates that participants could recognize changes in frequency and intensity over the experimented ranges.

TABLE II
RECOGNITION RATE FOR CHANGES IN FREQUENCY AND INTENSITY.

	Average	Standard Deviation
Intensity	76.5%	2.52%
Frequency	77.77%	3.46%

The results can be further analyzed by exploring the average score of the users to the individual transitions. Tables III and IV show the average recognition rates for the different transitions for frequency and intensity respectively, along with the corresponding standard deviations. The lowest score for intensity transition recognition is 60% for intensity transitions from medium to high. This suggests that as the intensity of vibration increases, the ability for humans to distinguish changes of these intensities decrease. As for the frequency changes, the lowest recognition rate was medium to low at a rate of 58%. It seems that, on contrary to intensity, as the frequency of vibration decreases, the ability of humans to distinguish changes in frequency decreases.

TABLE III
RECOGNITION RATE FOR INTENSITY CHANGE

Intensity	Low	Medium	High
Low	67%	73%	93%
Medium	91%	60%	60%
High	98%	69%	78%

Finally, the response time of each participant was recorded, averaged and plotted against each trial for the intensity and the frequency variations. The results are shown in Figures 10 and 11 respectively. Both figures show that the average response time is higher at the beginning of the experiment, then is reducing quickly and stabilizes after around 7 trials. This implies that participants could easily and quickly learn various vibrotactile cues that are generated by combinations of frequency and/or intensity of the stimulation.

TABLE IV
RECOGNITION RATE FOR FREQUENCY CHANGE

Frequency	Low	Medium	High
Low	78%	60%	88%
Medium	58%	84%	91%
High	86%	80%	73%

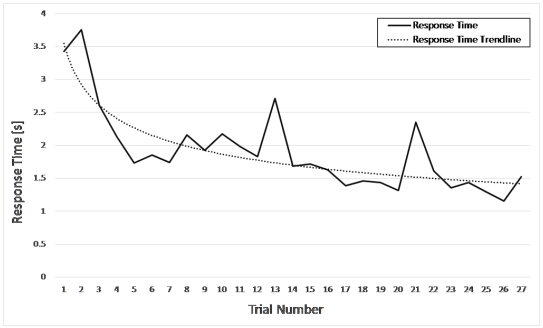

Fig. 10. The average response time for each repetition in the intensity change part of the study

VI. DISCUSSION

The magnetostatic analysis and the frequency response analysis showed that it is possible to create a simulation-based design of a vibrotactile actuator, whereas by changing different parameters, such as size of coil or shape of the magnet (in the case of the magnetostatic analysis) and diameter of the actuator or the thickness of the membrane (in the case of frequency response analysis), it is possible to tune the actuator

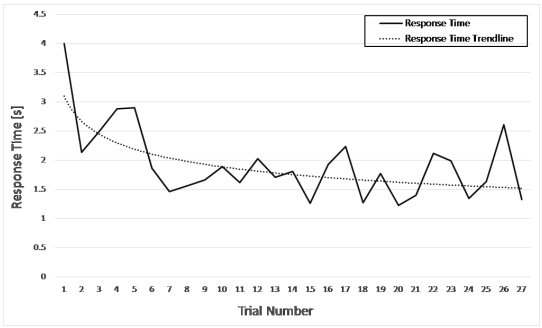

Fig. 11. The average response time for each repetition in the frequency change part of the study

for different intensity levels or frequency bands. This design process must be guided by the application needs.

The characterization method showed that it is possible to accurately match the characterization properties as shown theoretically through the simulation. The lack of a laser vibrometer or a relevant instrument capable of measuring the exact displacement of the actuator was compensated by the accelerometer, which was attached to the surface of the actuator. This turned out to work well since the results derived from the experimental study matched those obtained in the simulation. The frequency response curve was also extended for a variety of different voltages which consist the working space of the actuator. By using the 3D surface plot of Figure 8 as a mapping function one can use the actuator to create stimulation patterns in a wide range of frequencies and intensities. The ability to independently control frequency and intensity of vibration enables the construction of a flat-response actuator along either frequency or intensity. The transient response of the actuator showed that the actuator is suitable for real-time applications.

The perceptual characterization study offered the perceptual mappings of frequency/intensity changes, given that this actuator is designed to provide high expressivity of vibrotactile cues in wearable applications. More specifically, the study reveals that the users can easily distinguish changes in the vibration intensity and frequency with a high recognition rate. Our results suggest that as the intensity increases, the ability of humans to perceptually distinguish changes decreases, probably because of the vibrotactile saturation effect [18]. On the other hand, results demonstrated that as the frequency decreases, changes become harder to distinguish. This is in line with previous research studies referring to the decline in perceptual recognition as the frequency of vibrotactile stimulation decreases [19]. Finally, a learning phase is observed at the initial trials of the experiment whereas the average recorded response time was higher for both intensity and frequency studies but it rapidly decreases and stabilized as the experimental trials advance. Participants quickly and accurately learned the vibrotactile cues.

VII. Conclusion

This paper presented the design, implementation, characterization, and perceptual evaluation of a low-profile vibrotactile actuator that is capable of controlling frequency and intensity of vibration independently. The actuator outperforms ERM and LRA actuators in terms of control space. Also, its cost is an order of magnitude less than voice coil based tactile actuators. As for future work, we plan to develop an array of these actuators in order to develop a haptic jacket capable of simulating apparent tactile stimulation. Another follow-up psychophysical study will also be conducted with the jacket to verify the ability of the actuator to simulate apparent tactile motion.

References

[1] Y. Zheng and J. B. Morrell, "Haptic actuator design parameters that influence affect and attention," in *Haptics Symposium (HAPTICS), 2012 IEEE*. IEEE, 2012, pp. 463–470.

[2] S. Brewster, S. Brewster, F. Chohan, and L. Brown, "Tactile feedback for mobile interactions," in *Proceedings of the SIGCHI conference on Human factors in computing systems*. ACM, 2007, pp. 159–162.

[3] M. Hafez, "Tactile interfaces: technologies, applications and challenges," *The Visual Computer*, vol. 23, no. 4, pp. 267–272, 2007.

[4] V. G. Chouvardas, A. N. Miliou, and M. K. Hatalis, "Tactile displays: Overview and recent advances," *Displays*, vol. 29, no. 3, pp. 185–194, 2008.

[5] G. Korres and M. Eid, "Haptogram: ultrasonic point-cloud tactile stimulation," *IEEE Access*, vol. 4, pp. 7758–7769, 2016.

[6] P. Rizun and G. Sutherland, "Tactile feedback laser system," Sep. 21 2006, uS Patent App. 11/261,445.

[7] R. W. Lindeman, Y. Yanagida, H. Noma, and K. Hosaka, "Wearable vibrotactile systems for virtual contact and information display," *Virtual Reality*, vol. 9, no. 2-3, pp. 203–213, 2006.

[8] E. T. Kern, "Engineering haptic devices," *New York: Springer-Verlag*, 2009.

[9] H.-Y. Yao and V. Hayward, "Design and analysis of a recoil-type vibrotactile transducer," *The Journal of the Acoustical Society of America*, vol. 128, no. 2, pp. 619–627, 2010.

[10] Y. Y. S. C. W. Park, T. Yang and S. Kim, "Flexible and bendable vibrotactile actuator using electro-conductive polyurethane," *2015 IEEE World Haptics Conference (WHC)*, pp. 165–170, 2015.

[11] C. A. C. E. J. J. H. Huang, T. Li and V. M. Koch, "Experiment and investigation of two types of vibrotactile devices," *2016 6th IEEE International Conference on Biomedical Robotics and Biomechatronics (BioRob)*, pp. 1266–1271, 2016.

[12] M. E. A. El Saddik, M. Orozco and J. Cha, "Haptics technologies: Bringing touch to multimedia," *New York: Springer-Verlag*, 2011.

[13] S. Choi and K. J. Kuchenbecker, "Vibrotactile display: Perception, technology, and applications," *Proceedings of the IEEE*, vol. 101, no. 9, pp. 2093–2104, 2013.

[14] W. McMahan and K. J. Kuchenbecker, "Dynamic modeling and control of voice-coil actuators for high-fidelity display of haptic vibrations," *2014 IEEE Haptics Symposium (HAPTICS)*, pp. 115–122, 2014.

[15] B. J. Mortimer, G. A. Zets, and R. W. Cholewiak, "Vibrotactile transduction and transducers," *The Journal of the Acoustical Society of America*, vol. 121, no. 5, pp. 2970–2977, 2007.

[16] K. Parsons and M. Griffin, "Whole-body vibration perception thresholds," *Journal of Sound and Vibration*, vol. 121, no. 2, pp. 237–258, 1988.

[17] Y. Matsuura, S. Okamoto, and Y. Yamada, "Estimation of finger pad deformation based on skin deformation transferred to the radial side," in *International Conference on Human Haptic Sensing and Touch Enabled Computer Applications*. Springer, 2014, pp. 313–319.

[18] V. Duthoit, J.-M. Sieffermann, E. Enrègle, and D. Blumenthal, "Perceived intensity of vibrotactile stimuli: Do your clothes really matter?" in *Proceedings, Part I, of the 10th International Conference on Haptics: Perception, Devices, Control, and Applications - Volume 9774*, ser. EuroHaptics 2016. Springer-Verlag, 2016, pp. 412–418.

[19] M. Hollins and E. Roy, "Perceived intensity of vibrotactile stimuli: the role of mechanoreceptive channels," *Somatosensory And Motor Research*, vol. 13, no. 3, pp. 273–286, 1996.